SOLIDIFICATION INDUCED THERMOELASTIC FRAGMENTATION DURING FCI

B.Ghosh, D.Mukhopadhyay and H.G.Lele
Reactor Safety Division, Bhabha Atomic Research Centre, Mumbai, INDIA-400085
E-mail of corresponding author: bghosh@barc.gov.in

ABSTRACT

Solidification induced thermoelastic stresses and related pressure fields play an important role in the fragmentation of molten fuel during fuel-coolant interaction in severe accidents of nuclear reactors. Here we have analyzed the solidification behaviour and temperature field within the solidified shell of spherical molten fuel drops. The resulting temperature distribution has been used to evaluate the thermoelastic stress field within the solidified shell. The compression of the melt-core and its effect on the overall stress field has been considered. The fuel-coolant combinations we have studied are UO_2-Na and Al-H_2O systems. Two approximate analytical (existing quasi-steady and integral equation with successive approximation that is derived here) approaches and enthalpy-based numerical methods have been used for these analyses. Relative merits of the analytical approaches have been explored. The maximum values of solidification induced stresses have been noted to be sufficient for fuel fragmentation.

INTRODUCTION

During the course of severe accident, a molten fuel coolant interaction (MFCI) may occur. During MFCI molten jet and drop may fragment into particles. The process of this interaction can range from benign film boiling, drop fragmentation due to relative motion, solidification crust formation and further prevention of fragmentation, to more destructive pressure wave propagation and explosive interactions. The drop fragmentation process is responsible for interfacial area evolution during the premixing and propagation phases of steam explosion. More importantly, in non-explosive situation, configurations of particles (size distribution, porosity, etc.) are critical to the coolability of the debris bed generated during this process. Fragmentation modeling of melt droplets is essential for numerical study of FCIs which are important in nuclear reactor severe accident analysis.

Existing fragmentation models can be classified as: (1) those based on *hydrodynamic* effects between the molten material and coolant, independent of the thermal condition; (2) *vapour film* models, which assume that the fuel undergoes fragmentation due to pressure forces initiated due to growth and collapse of coolant vapour film; (3) violent *gas release* models, which postulate the breakup under the 'latent pressure' of dissolved gases in the molten material and escaping under cooling; (4) solid shell theories, which consider thermal cooling effects and surface solidification (Cronenberg [1975]).

Brauer et al. [1968] did an experiment on a single droplet FCI, in which an aluminum or a lead droplet was released into water. The results showed that the molten aluminum appeared to had been forced through a porous solid exterior shell and the molten lead was violently ejected from the original droplet, revealing the existence of the internal pressure inside the melt droplet. Hsiao [1972] and Witte [1973] analyzed the heat transfer process during solidification, calculated the thermal stress using elasticity theory for the case of aluminum quenched in water, and indicated that the *tangential stress* primarily induced by solidifying shell is dominant in the rupture of the shell. Cronenberg et al. [1974] studied the fragmentation process of molten UO_2 upon contact with sodium coolant and concluded that thermal stress in the outer shell and pressurization of the inner molten core induces fragmentation.

Here we develop approximate analytical models for analyses of solidification rate and resulting thermo-elastic stress field. The predictions of the analytical models have been validated against an enthalpy-based numerical model. Table 1 shows the data relevant for FCI analyses of UO_2-Na and Al-H_2O systems.

Table 1: Relevant Properties for FCI Analysis

Fuel	UO_2	Al
k (cal/sec-cm-^{o}C)	0.005	0.347
ρ_s (gm/cm^3)	11	2.7
c_p (cal/g-^{o}C)	0.11	0.26
T_f (^{o}C)	2800	660
L (cal/g)	67	95.4
E (psi)	26.5×10^6 $(1 - 0.6T/2700)$	4×10^6
K (psi)	4×10^6	11.5×10^6
ε (cm/cm-^{o}C)	1.8×10^{-6} $(4.2 + 2.8/2000)$	10.8×10^{-6}
ν	0.5	0.5
Coolant	Na	H_2O
k (cal/sec-cm-^{o}C)	0.184	0.00143
ρ (gm/cm^3)	0.896	1.0
c_p (cal/g-^{o}C)	0.3	1.0
T_c (^{o}C)	200-450	20.0
ρ_i (g/cm^3)	8.74	---
T_i (^{o}C)	945	615

HEAT TRANSFER CONTROLLED SOLIDIFICATION CALCULATION

The idealized problem of FCI for a corium droplet can be defined as a molten isotropic spherical droplet suddenly immersed in a homogeneous infinite cooling medium. It is assumed that the initial temperatures are such that, upon contact, the material begins to solidify in the outer shell, where a temperature gradient is established resulting in thermal stresses and pressurization of the inner molten core. The assumption of solidification is based on crystallization kinetics calculations (Cronenberg & Fauske [1974]) which indicate that the time for molecular re-ordering to form solid from the melt is short compared to the time constant for heat transfer.
Using constant thermophysical properties, the Fourier heat conduction equation for spherical geometry is

$$\frac{\partial T}{\partial t} = \frac{\alpha}{r^2}\frac{\partial}{\partial r}\left(r^2 \frac{\partial T}{\partial r}\right) \tag{1}$$

This equation and subsequent analysis is based on the following assumptions:
(1) Solidification for the liquid case is instantaneous; (2) Compressibility is neglected; (3) Densities of both phases of the fuel are assumed the same; (4) The transition temperature from liquid to solid UO_2 is at fixed at temperature of 3073 K; (5) Fission product decay heat in the fuel is neglected.

The definition of the above conductive heat transfer problem is complete with specification of the related initial and boundary conditions as described below.
The molten drop is assumed to be initially at the saturated freezing temperature,

$$T(r, 0) = T_f. \tag{2}$$

At the melt-solid interface, the two conditions to be satisfied are the energy balance at the interface, Stefan condition

$$\rho L_f \frac{\mathrm{d}R_i}{\mathrm{d}t} = k\frac{\partial T}{\partial r}\bigg|_{r=R_i} \tag{3}$$

and temperature continuity condition,

$$T(R_i, t) = T_f. \tag{4}$$

At the surface of the spherical drop, two possible alternative boundary conditions are: (1) convective Newtonian cooling and (2) perfect wetting temperature. The mathematical representations of these boundary conditions are listed below.

***Convective Boundary Condition*:** Under this condition the boundary condition at the outer surface of the droplet can be expressed

$$-k\frac{\partial T}{\partial r}\bigg|_{r=R} = h\big(T(R) - T_e\big) \tag{5}$$

where h depends on the surface heat transfer mode (i.e., pre- or post-CHF).
By virtue of flux continuity condition at unknown melt-solid interface, above relations constitute a nonlinear system of equations for temperature, T and solid shell thickness δ.

***Wetting Boundary Condition*:** An alternate surface boundary condition may exist if perfect wetting occurs. Based on a compilation of contact angle measurements between UO_2 and liquid metals, including sodium, Eberhart [1973] concludes that at the elevated temperatures experienced in reactor safety tests wetting of either solid or molten UO_2 can be expected. Therefore, as a result of such contact an interface temperature at the surface of separation will be established instantaneously according to Carslaw & Jaeger [1959].

$$T_i = \frac{T_H\sqrt{(\rho C_p k)_H} + T_C\sqrt{(\rho C_p k)_C}\ \mathrm{erf}(\lambda)}{\sqrt{(\rho C_p k)_H} + \sqrt{(\rho C_p k)_C}\ \mathrm{erf}(\lambda)} \tag{6}$$

where the subscripts H and C refer to the hot and cold substances respectively. λ is determined from the following transcendental equation assuming the UO_2 liquid is originally at its melting point:

$$\left.\frac{C_p T_m}{\sqrt{\pi} L}\right|_{\mathrm{UO_2}} = \lambda\, \mathrm{e}^{\lambda^2}\left(\frac{\sqrt{(\rho C_p k)_H}}{\sqrt{(\rho C_p k)_C}} + \sqrt{(\rho C_p k)_C}\ \mathrm{erf}(\lambda)\right) \tag{7}$$

For the bulk of UO_2 at its melting temperature of 3073 K and sodium at 473 K, $\lambda \approx 0.94$, and the interfacial temperature is 945°C (Cronenberg [1974]).
The boundary condition for this case is the isothermal condition given by,
$T(R_i, t) = T_i$. (8)

The final relation required to close the moving interface conduction problem is the initial interface location, that is,
$r(0) = R$. (9)

The nonlinearity of Stefan condition () embodies the difficulty in solving the problem. For spherical geometry only a limited number of solutions are available, such as that by Langford [1966] for a specified solidification rate and the steady-state approximation of Landon and Seban [1943] used by Langford [1966]. Adams [19581 developed a solution for a constant surface temperature by transforming the partial differential boundary-value problem into an integral equation and solving by successive approximations. Here we have developed an improved approximate solution for convection cooling condition. Adam's solution can be derived as an asymptotic limit of Bi $\to \infty$ from the present solution. In order not to neglect the transient nature of the solidification process, an enthalpy-based numerical solution of equations (1) though (4), equation (5) or (8), and equation (9) has been obtained.

Quasi-Steady Approach
A simplified model for temperature distribution may be obtained through solution of the quasi-steady state conduction equation which results after omission of transient term in the governing differential equation (). The explicit time dependence in auxiliary relations, if any, is retained.

***For Convective Cooling*:** For the case of convective cooling the temperature distribution is evaluated as,
$\theta = (\eta/\xi)(1-\beta\xi)/(1-\beta\eta)$ (10)

where $\theta = (T - T_e)/(T_f - T_e)$, $\xi = r/R$, $\eta = R_i/R$, Bi = hR/k, and $\beta = 1 - 1/\mathrm{Bi}$.
T monotonocally reduces from T_f to $T(r = R)$. As Biot number, Bi, increases larger part of the temperature drop takes place within the solidified shell. As $R_i \to 0$, $T(R) \to T_e$.

The evolution of thickness of the crust can be found from the heat balance relation,

$$(1-\eta)\left\{\frac{1}{2}(1+\eta) - \frac{\beta}{3}\left(1+\eta+\eta^2\right)\right\} = \tau \tag{11}$$

where normalized time, $\tau = k(T_f - T_e)t/(\rho L_f R^2) = \mathrm{St}_e \alpha t / R^2$
This relation is identical to that derived by London & Seban [1943] with a thermal circuit analysis. For practically relevant high values of Biot number, the history of growth of shell thickness becomes effectively independent of Bi number.

For Perfect Contact: Under perfect wetting condition, the corresponding relations for temperature evolution and interface movement are given by,
$\theta = (\eta/\xi)(1-\xi)/(1-\eta)$ (12)
and $\eta^3 - \frac{3}{2}\eta^2 - \frac{1}{2}(6\tau - 1) = 0$ (13)

It is to be noted here that normalized variable are independent of Stefan number. Moreover, the above relations (12) and (13) can be derived from the corresponding relation (10) and (11) for convective cooling as a limit of $\beta \to 1$.

Integral Equation Approach
In this approach we have integrated the heat conduction equation (1) with respect to the space variable and used the Stefan condition (3) and replace the term explicit in time variable with the instantaneous interface location. This leads to an integral equation for temperature gradient. Nest, judiciously using the relations derived in the quasi-

steady approach and integrating further and using the interfacial temperature boundary condition (4), we obtain a temperature distribution in terms of the velocity of interface. Finally, using the surface boundary condition (5) or (8), we arrive at a nonlinear first-order ordinary differential for the interface movement. Integration of this relation (analytically or numerically) with initial condition (9) yields the requisite relation for thermal analysis.

For Convective Cooling: Using above procedure, we have derived the improved approximate solution, starting from the above quasi-steady solution, consisting of the following relations:

$$\theta = 1 + \eta \frac{\xi - \eta}{\xi} \frac{\mathrm{d}\eta}{\mathrm{d}\tau} \left\{ 1 - \mathrm{St}_e \frac{\mathrm{d}\eta}{\mathrm{d}\tau} \frac{\xi - \eta}{1 - \beta\eta} \left(\frac{1}{2} - \beta \frac{\eta}{3} - \beta \frac{\xi}{6} \right) \right\} \tag{14}$$

and $$\frac{\mathrm{d}\tau}{\mathrm{d}\eta} = -\frac{1}{2}\eta(1-\beta\eta)\left[1 + \sqrt{1 + \frac{4\mathrm{St}_e}{3\beta} \frac{1}{\eta} \left\{ 1 - \frac{(1-\beta)^3}{(1-\beta\eta)^3} \right\}} \right] \tag{15}$$

For Perfect Contact: In the limiting case of Bi $\to \infty$ (i.e., $\beta \to 1$), the equation (14) and (15) reduces to

$$\theta = 1 + \eta \frac{\xi - \eta}{\xi} \frac{\mathrm{d}\eta}{\mathrm{d}\tau} \left\{ 1 - \mathrm{St}_s \frac{\mathrm{d}\eta}{\mathrm{d}\tau} \frac{\xi - \eta}{1 - \eta} \left(\frac{1}{2} - \frac{\eta}{3} - \frac{\xi}{6} \right) \right\} \tag{16}$$

and $$\frac{\mathrm{d}\tau}{\mathrm{d}\eta} = -\frac{1}{2}\eta(1-\eta)\left(1 + \sqrt{1 + \frac{4}{3}\frac{\mathrm{St}_s}{\eta}} \right) \tag{17}$$

which are equivalent to relation developed by Adams [1958] for a constant surface temperature.
In the present study, equation (14), (16) and (17) have been evaluated in closed form analytical form, whereas equation (15) has been resolved through numerical integration.

Enthalpy-Based Numerical Method

The essential feature of the basic enthalpy methods is that the evolution of the latent heat is accounted for by the enthalpy as well as the relationship between the enthalpy and temperature. The relationship between the enthalpy and temperature can be defined in terms of the latent heat release characteristics of the Phase-Change Material (PCM). This relationship is usually assumed to be a step function for isothermal phase change and a linear function for nonisothermal phase-change cases. There is extensive literature on the application of various versions of the enthalpy method for phase-change problems.
Here, the variant of enthalpy method harnessed here for numerical modeling of solidification of spherical drop is an extension of generalized method introduced by Date [1991] to spherical geometry.
In this method suitably normalized temperature is expressed as sum of normalized enthalpy and a correction term as,

$$\theta = \phi + \theta' \tag{18}$$

The heat conduction equation thus can be expressed as,

$$\frac{\partial \phi}{\partial \tau} = \frac{1}{\xi^2} \frac{\partial}{\partial \xi} \left(\xi^2 \frac{\partial \phi}{\partial \xi} \right) + \frac{1}{\xi^2} \frac{\partial}{\partial \xi} \left(\xi^2 \frac{\partial \theta'}{\partial \xi} \right) \tag{19}$$

The temperature correction is related to enthalpy as,

$$\theta' = \tfrac{1}{2}\left(-\phi - |\phi| \right) + \tfrac{1}{2}\left(\phi - 1 + |\phi - 1| \right) = \tfrac{1}{2}\left(|\phi - 1| - |\phi| - 1 \right) \tag{20}$$

Since ϕ represents the liquid fraction, $1 - \phi$ or $1 + \theta'$ represents the solid fraction.
The governing equations listed above have been discretised implicitly. The resulting algebraic equations have been solved by using TDMA algorithm. The values of the dimensionless quantities such as Stefan number and Biot number have been taken from the table 1.

Results of Solidification Calculation

In UO_2-Na system, the molten UO_2 is assumed to be initially at saturation temperature of 3073 K. For convective cooling mode, the nucleate boiling heat transfer coefficient for UO_2-Na system is taken as 5.677×10^4 W/m^2/K at the coolant (Na) temperature of 473 K. The choice of nucleate boiling over film boiling was based upon Henry's [1973] correlation which indicates that for 473 K Na the minimum temperature for film boiling is about 9773 K. This suggests that even after solidification some contact exists and if boiling occurs, it is in the nucleate or transition

regimes. For perfecting wetting mode, the interface temperature is kept fixed at contact temperature 1218 K as obtained from equations (6) and (7).

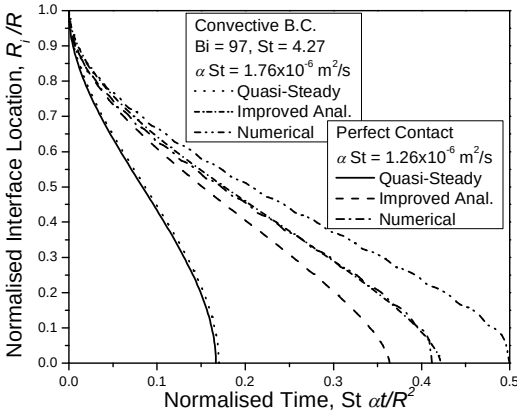

Fig.1: Freezing Rate in the UO_2-Na Systems

Figure (1) represents growth rates as predicted by different approaches, under convective cooling condition for fuel-coolant systems chosen here. As specific area tends to infinity with the radius of the molten core reducing to zilch, the rate of solidification approaches an unbounded rate. When compared to numerical solution, the accuracy of the improved approximate solution is superior to that of quasi-steady one. Owing to low thermal conductivity (high Biot number) of UO_2, solidification process is essentially limited by the conductivity rather than the surface heat transfer process. As a consequence, growth rates predicted by quasi-steady approach are very nearly same for convective cooling and perfect contact conditions. Though these rates are quite different (fast) compared to other estimation methods, effect of boundary conditions on the actual rate of solidification is not very prominent.

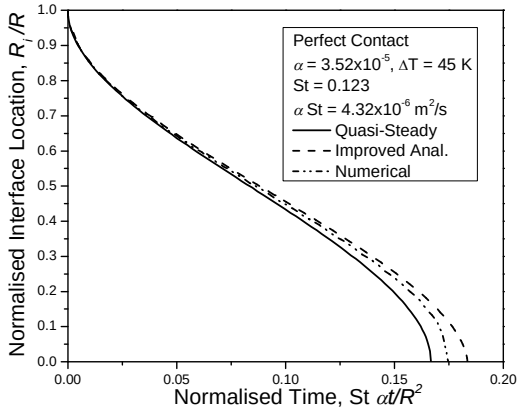

Fig.2a: Solidification in Al-H_2O System (Wetting)

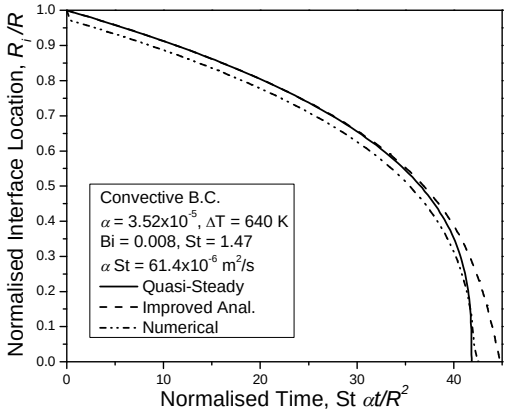

Fig.2b: Solidification in Al-H_2O System (Convection)

In Al-H_2O system, the molten Al is assumed to be initially at saturation temperature of 923 K. For perfecting wetting mode, the interface temperature is kept fixed at the contact temperature 888 K as obtained from equations (6) and (7). In this case, the initial temperatures of the system are such that the aluminum surface temperature (888 K is significantly higher than the minimum wall temperature (508 K) to sustain film boiling (Baumeister et al. [1969]). As a consequence, for convective cooling mode, the film boiling heat transfer coefficient for Al-H_2O system is taken as 2.261×10^2 W/m^2/K at the coolant (H_2O) temperature of 293 K.

Growth rates for different cooling modes are plotted in figures (2a) and (2b). The solidification process for the highly conductive (low Biot number) aluminum is strongly dependent upon the surface heat transfer process. Even though, temperature difference is larger for convective cooling (larger Stefan number), due to low heat transfer coefficient in the film boiling regime, a comparison of figures (2a) and (2b) reveals that the solidification rate in convective condition is an order-of-magnitude lower than the perfect contact condition.

Since the Fourier number for aluminum is much greater than that for uranium-oxide ((Fo(Al)/Fo(UO_2) ~ 85), the effect of neglecting the thermal inertia term is not as critical for the highly conductive aluminum as it is for UO_2. Thus, the solutions obtained through quasi-steady approach bear reasonably agreement with enthalpy-based numerical method.

THERMOELASTIC STRESS, PRESSURIZATION AND FRAGMENTATION ANALYSES

As we have seen above, when the liquid or the solid particle of fuel is immersed in the coolant an uneven temperature distribution is established within the solid portion. Because of this the cooler, more dense solid material at the surface attempts to contract but is constrained by the hotter less dense interior portion of the solid. This introduces a tensile stress at the surface of the

sphere and a compressive stress in the interior. In addition, the solid shell of the liquid drop and the totally solid drop attempt to contract radially inwardly due to these thermal stresses as well as the differential in temperature from its initial state. This behavior is more pronounced in the liquid due to the phase change. The liquid core has limited compressibility and the pressure within it rises, inducing secondary pressure stresses both radially and tangentially.
The analytical model for solidification on the surface of a molten drop, is employed to calculate the pressure generation during the solidification. It is assumed that the solidification progresses spherically inwards. At the interface between solid shell and the molten material within it, the temperature is assumed to be always equal to the freezing temperature (T_f), while the temperature outside the crust is much below it. Due to temperature distribution within the solid shell, the thermal stresses are generated.

Thermo-Elastic Stress Analysis
Considering the molten droplet to be an isotropic elastic sphere, with the origin of spherical coordinates at the center of the sphere, subjected to spherically symmetrical external tractions and spherically symmetrical temperature field $T = T(r)$, the thermo-elastic stress field in solidified spherical shell is given by

$$\sigma_r^{(t)}(r) = 2\frac{\varepsilon E}{1-\nu}\frac{1}{r^3}\left\{\frac{r^3 - R_i^3}{R^3 - R_i^3}\int_{R_i}^{R}\left(T - T_f\right)r^2\,\mathrm{d}\,r - \int_{R_i}^{r}\left(T - T_f\right)r^2\,\mathrm{d}\,r\right\} \tag{21a}$$

$$\text{and } \sigma_\theta^{(t)}(r) = \frac{\varepsilon E}{1-\nu}\left\{\frac{2r^3 + R_i^3}{R^3 - R_i^3}\frac{1}{r^3}\int_{R_i}^{R}\left(T - T_f\right)r^2\,\mathrm{d}\,r + \frac{1}{r^3}\int_{R_i}^{r}\left(T - T_f\right)r^2\,\mathrm{d}\,r - \left(T - T_f\right)\right\} \tag{21b}$$

where $\sigma_r^{(p)}$ and $\sigma_\theta^{(p)}$ are the thermal stresses in radial and circumferential direction.

Melt-Core Pressurization and Stresses in Shell
Here it is assumed that, in addition to a steady-state radial temperature gradient, the spherical shell is traction free and is submitted to an action of an internal *uniform pressure* P_i, in the molten core.
The solid shell compresses the liquid residing inside it. In the other words, the pressurization on the interface is induced during the solidification. It also needs to be noted that the compressive strain on inner and outer face of the cell are equal. Moreover, unlike stresses, strains depend on initial temperature. The stresses due to pressurization (Roak and Young [1976]), can be expressed through the following relations,

$$\sigma_r^{(p)} = -\frac{R^3 - r^3}{R^3 - R_i^3}\frac{R_i^3}{r^3}P_i \quad \text{and} \quad \sigma_\theta^{(p)} = \frac{1}{2}\frac{2r^3 + R^3}{R^3 - R_i^3}\frac{R_i^3}{r^3}P_i \tag{22a, b}$$

where $\sigma_r^{(p)}$ and $\sigma_\theta^{(p)}$ are the stresses in radial and circumferential direction due to pressurization inside the droplet and P_i is the pressure.

Net Pressure and Stress Fields
It is assumed that the compressibility of melt is negligibly small ($\partial\rho/\partial p$ of the melt is very small, and the corresponding contribution to displacement of the shell is small). The resulting *radial displacement* at the interface due to thermal stresses and that due to internal pressure should go to zilch, and using the condition $T(r = R_i) = T_f$, we arrive at the relation,

$$P_i = \frac{6\varepsilon E}{2(1-2\nu)R_i^3 + (1+\nu)R^3}\int_{R_i}^{R}\left\{T_0 - T(r)\right\}r^2\,\mathrm{d}\,r \tag{23}$$

Finally the net stress field in the spherical shell is given by,

$$\sigma_r(r) = \sigma_r^{(t)} + \sigma_r^{(p)} \quad \text{and} \quad \sigma_t(r) = \sigma_t^{(t)} + \sigma_t^{(p)} \tag{24a, b}$$

Results of Thermoelastic Calculations:
Relations (22) through (24) have been evaluated analytically as a closed form algebraic solution using the temperature distribution obtained from equations (14) and (16). The thermo-mechanical data presented in table 1 has been used wherever necessary for generation of numerical data are required from these closed form solutions.
Figure (3) shows the variation of pressure with growth of solidified shell under two different boundary conditions with different analytical approximations. The pressurization predicted by quasi-steady and improved approximation is in reasonable agreement. The discrepancies increase with progress of solidification. Pressure profiles, predicted by quasi-steady model, increase monotonically right upto the end of solidification process; whereas predictions by

improved approximation exhibit decrease towards the end of freezing. This is more prominent in convective cooling condition of Al-H_2O. This may be attributed to corresponding slower rate of freezing as evident in figure (2b).

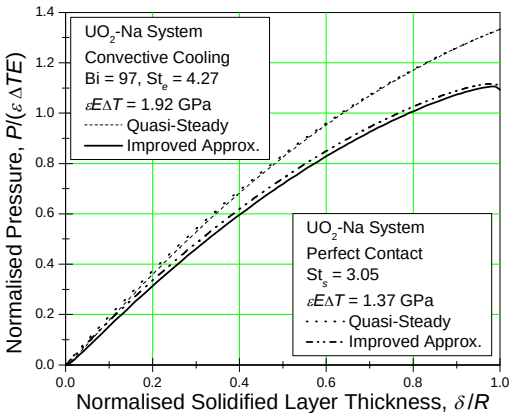

Fig.3a: Pressurization in the UO_2-Na System

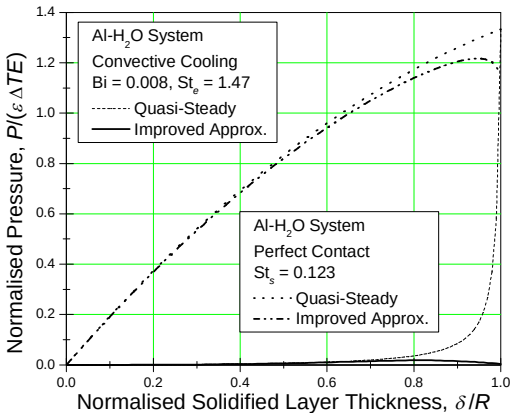

Fig.3b: Pressurization in the Al-H_2O System

Figures 4a and 5a show that the magnitude of radial thermal stress possesses a maximum at the interior of the solidified shell and this maximum value increases as the solidification progresses. The circumferential thermal stress increases monotonically from a negative value at the freezing interface to a positive value at the free surface. The magnitude of the negative maximum increases whereas that of positive maximum decreases with solidification. Improved approximation predicts radial stresses with slightly larger magnitudes for Al-H_2O system. For circumferential stresses, it predicts lower magnitude of negative maximum but higher magnitude of positive maximum for the same system for perfect wetting case, but both of these are lower for convective cooling case.

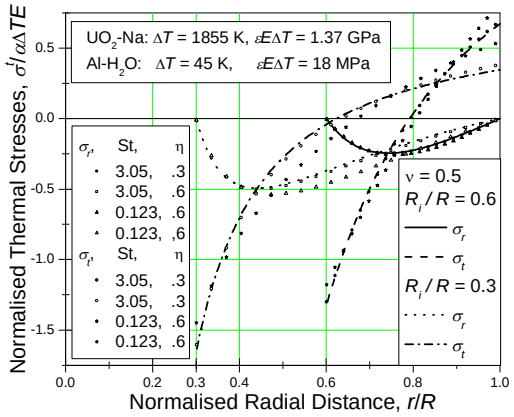

Fig.4a: Thermal Stresses for Perfect Wetting Case

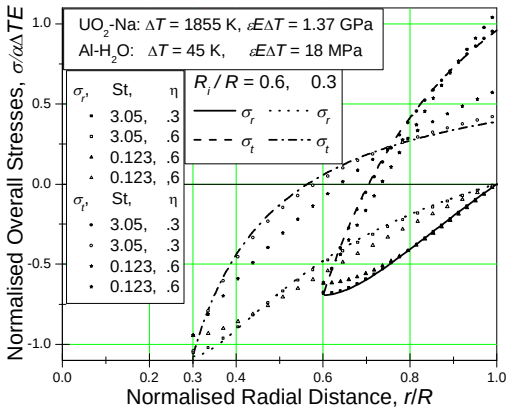

Fig.4b: Overall Stresses for Perfect Wetting Case

Figure 4b and 5b reveal that the radial overall stress also varies monotonically and it magnitude reaches at a maximum at the freezing front. The magnitude of this maximum increases as the freezing front moves inwards.

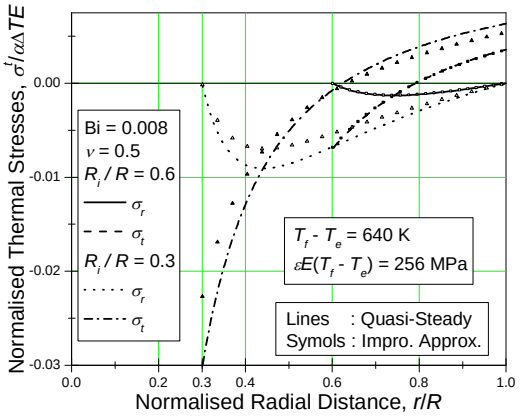

Fig.5a: Thermal Stresses for Al (Convective Case)

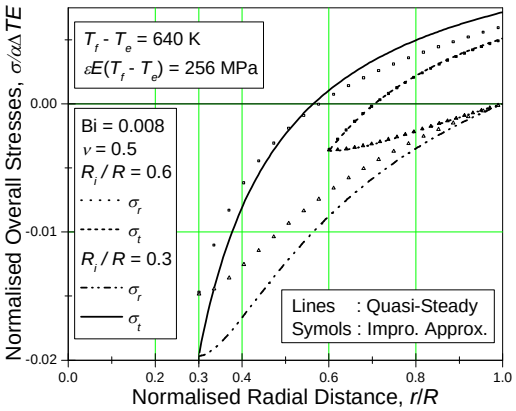

Fig.5b: Overall Stresses for Al (Convective Case)

The maximum negative value of circumferential stress at interface is same as that of radial stress (for $\nu = ½$!).
As it is evident from figure 6a-c, the circumferential stress at the free surface decreases monotonically with solidification for the perfect contact condition, it reaches a maximum a short time after beginning of the solidification for the UO_2-Na system under convective cooling and towards the end of the solidification process for Al-H_2O system under convective cooling. In consonance previous discussion on relative prediction of improved approximation approach, the maximum value of surface stress is slightly larger for perfect contact condition, but smaller for convective cooling cases. It is notable (in figure 6c) for the Al-H_2O system. It also leads to early occurrence of maximum value of surface circumferential stress. In all cases, quasi-steady approach predicts vanishing surface stress at the final moment of the solidification process, whereas improved approximation predicts finite residual thermal and total surface stresses. The discrepancy has the origin at the erroneous near-singular temperature profile predicted by quasi-steady approach near the final phase of solidification event.

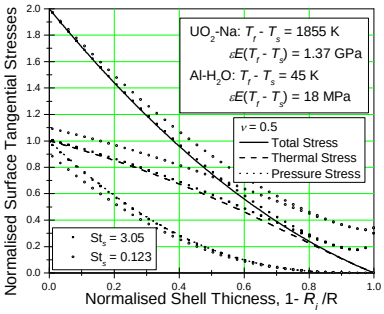

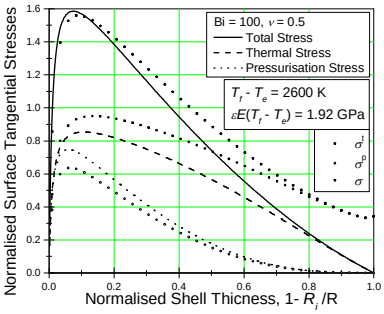

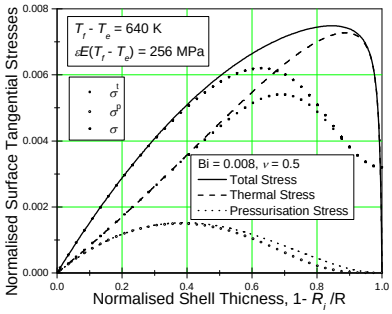

Fig.6a: Surface Stresses (Wetting) **Fig.6b: UO_2 Surface Stresses (Conv.)** **Fig.6c: Al Surface Stresses (Conv.)**

For Al-H_2O system, magnitude of stress level for convective cooling is an order of magnitude less than that for perfect contact. For UO_2–Na system, under both heat transfer boundary conditions, the calculated stresses are an order of magnitude larger, than the yield strength of 34.5 MPa at 2273 K and sufficient for fragmentation.

CONCLUSION

Differences in Solidification behavior of spherical droplets in fuel-coolant systems of UO_2-Na and Al-H_2O under two possible cooling conditions due to substantial variation in fuel thermal conductivity have been captured through two approximate analytical approaches and an enthalpy-based numerical method. Relative predictions of the thermoelastic stresses through two analytical approaches have been pointed out and analyzed. The calculated solidification induced stress levels have been found to be high enough for fragmentation.

REFERENCES

[1] Adams, C.M. "Thermal Considerations in Freezing", *Liquid Metals & Solidification,* ASM, pp.187-217, 1958.
[2] Baumeister, K.J., Simon, F.E. and Henry, R.E. "Role of the Surface in Measurement of the Leidenfrost Temperature", *Proc. ASME Symp. Augmentation of Convective Heat and Mass Transfer,* pp., 1970.
[3] Brauer, F.E., Green, N.W. and Mesler, R.B. "Metal-Water Explosions", *Nucl. Sci. Eng.,* **31,** pp.551-4, 1968.
[4] Carslaw, H.S. and Jaeger, J.C. *Conduction of Heat in Solids,* Clarendon Press: Oxford, 1959.
[5] Cronenberg, A.W., Chawla, T.C. and Fauske, H.K. "A Thermal Stress Mechanism for the Fragmentation of Molten UO2 upon Contact with Sodium Coolant", *Nucl. Eng. Des.*, **30,** pp.434-43, 1974.
[6] Cornenberg, A..W. and Fauske, H.K. "UO_2 Solidification Phenomena Associated with Rapid Cooling in Liquid Sodium", *J. Nucl. Mater.*, **52,** pp.24-32, 1974.
[7] Cronenberg, A.W. and Grolmest, M.A. "Fragmentation Modeling Relative to the Breakup of Molten UO_2 in Sodium", *Nucl. Safety*, **16,** pp.683-700, 1975.
[8] Date, A.W. "A Strong Enthalpy Formulation for the Stefan Problem", *Int. J. HM T,* **34,** pp.2231-5, 1991.
[9] Eberhart, J. "The Wettability of Reactor Fuel by Molten Metals", *ANL-RDP-***22**, 7.26-7.28, 1973.
[10] Henry, R.E. "A Correlation for the Minimum Film Boiling Temperature", *Proc. AIChE HT Conf.*, pp., 1973
[11] Hsiao, K.H., et al. "Pressurization of a Solidifying Sphere", *J. Appl. Mech.*, **94,** pp.71-7, 1972.
[12] Langford, D. "The Freezing of Spheres", *Int. J. HMT*, **9,** pp.827-8, 1966.
[13] Landon, A.L. and Seban, R.A. "Rate of Ice Formation", *Trans. ASME*, **65**, pp.771-8, , 1943.
[14] Roark, R.J. and Young, W.C. *Formulas for Stress and Strain,* **5th ed.,** Mcgraw-Hill: Singapore, 1976.
[15] Witte, L.C. , Vyas, T.J. and Gelabert, A.A. "Heat Transfer and Fragmentation during Molten-Metal/Water Interactions", *J. Heat Transfer*, **95,** pp.521-7, 1973.